A Distortion Control Technique for Achieving High Power Efficiency in an HPA Array

Takana Kaho, Yoshinori Nakasuga, Hiroshi Okazaki, *Member, IEEE*, Katsuhiko Araki, and Kohji Horikawa, *Member, IEEE*

***Abstract*—This paper proposes a new technique for reducing the intermodulation (IM) distortion products in a high-power amplifier (HPA) array. The proposed technique dissolves the relations between carriers and IMs by applying IM phase control. As a result, IMs are distributed to all the output ports in the array, and the carrier power to intermodulation power ratio (C/IM) of the HPA array can be increased. The improvement in C/IM is as high as $10 \log N$ dB, where N is the number of HPAs. Newly developed even-order distortion implemented intermodulation distortion controllers (EODICs) are used to achieve the IM phase control. A test carried out using a four-parallel HPA array with EODICs confirms that the technique noticeably improves C/IM and demonstrates its validity.**

***Index Terms*—Intermodulation (IM) distortion, monolithic microwave integrated circuits (MMICs), power amplifiers, satellite communication onboard systems.**

I. Introduction

In MOBILE satellite communication systems, demands for high-speed access and large capacity are increasing due to the advent of the multimedia era. To achieve smaller earth station, such as handy phones, satellites are required to have highly effective isotropic radiated power (EIRP), and a high-power amplifier (HPA) with kilowatt-class RF power. One effective means of meeting these requirements is the use of an active phased-array antenna system (APAAS) with a large reflector [1].

Thermal loading becomes extremely large, however, in systems with kilowatt-class RF components. This is a serious problem for satellites that are poor at removing heat. Fig. 1 shows the relationship between power efficiency and thermal load required obtaining RF output power levels of 1–3 kW. The power efficiency of current on-board solid-state power amplifiers (SSPAs) is approximately 25% in the S- and C-bands [2], [3]. For example, it can be seen in Fig. 1 that to obtain RF output power of 2 kW using SSPAs that have 25% power efficiency, the thermal load is approximately 6 kW. To remove this thermal load, a satellite needs to be large in structure and has to have a large payload. This entails high costs and, thus, there is a need to greatly increase HPA efficiency.

Manuscript received May 11, 2001; revised December 26, 2001.

T. Kaho, Y. Nakasuga, and K. Araki are with the NTT Network Innovation Laboratories, Yokosuka 239-0847, Japan (e-mail: kaho@wslab.ntt.co.jp).

H. Okazaki is with the NTT Electronics Corporation, Machida 194-0004, Japan, on leave from the NTT Network Innovation Laboratories, NTT Corporation, Kanagawa 239-0847, Japan.

K. Horikawa is with the Radio Network Development Department, NTT DoCoMo Inc., Yokosuka 234-8536, Japan.

Digital Object Identifier 10.1109/TMTT.2002.804621

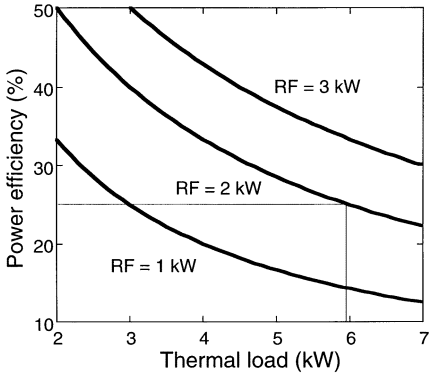

Fig. 1. Power efficiency versus thermal load of HPA.

In amplifiers, however, there is a tradeoff problem between efficiency and intermodulation distortion (IM). Since mobile satellite communication systems use multicarrier transmission, a high carrier power to intermodulation power ratio (C/IM) is required. To maintain the C/IM at the level the system requires, the output backoff (OBO) level must be several decibels lower than the output saturation point. In the near-saturated region, the power efficiency decreases by 5% for every 1 dB increase in the OBO level [3]. Any reduction in OBO with high C/IM is valuable in increasing HPA efficiency and, thus, reducing the thermal load. Many linearizers have been developed to compensate the nonlinear distortion at the OBO level of several decibels, but they are not strong enough to do so in the saturated regions [4]–[6].

To address this problem, we have briefly proposed a novel technique for reducing IM and creating a highly efficient HPA array [7]. This paper fully describes the principle of the technique and a developed IM controller, and shows experimental results obtained in applying IM control to an HPA and a four-element HPA array to confirm the basic function of the technique.

II. IM Control Technique

Our proposed IM control technique effectively reduces IMs; IM power is distributed, while carrier power is maintained. Figs. 2 and 3 explain the concept of this technique. In an HPA array, 3-dB 90° hybrid couplers are used as a divider matrix and a combiner matrix, as shown in Fig. 2. The signal launched at port IP_1 only appears (combines in-phase) at port OP_1 and cancels (combines out-of-phase) at ports OP_2–OP_4. Third-order intermodulations (IM3s) generated in each HPA with input to IP_1 are combined as same as carriers, then IM3s

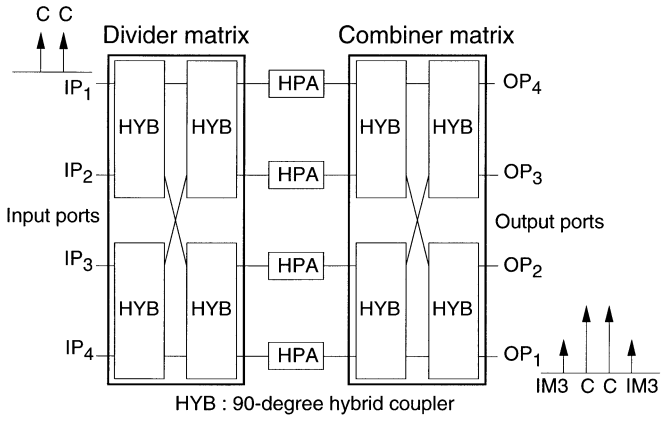

Fig. 2. Balanced HPA array. Arrows show the spectra in the frequency band.

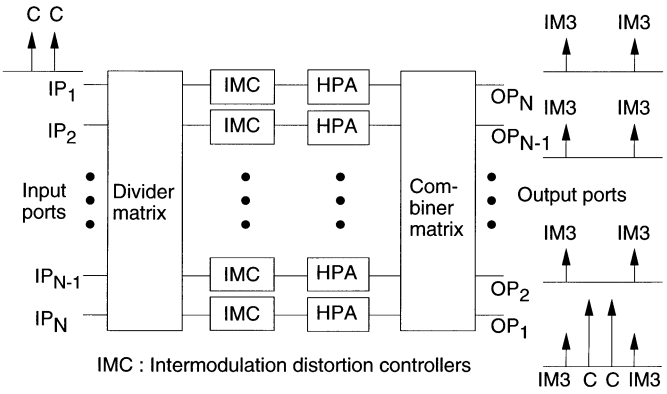

Fig. 3. Balanced HPA array with IM controllers. Arrows show the spectra in the frequency band.

appear at port OP_1 and do not appear at ports OP_2–OP_4. This is because there are relationships between the carriers and harmonics; therefore, IM3s behave the same with carriers. Such an operation requires perfectly balanced 3-dB 90° couplers and identical HPAs. The harmonics play the same if the couplers have a flat frequency response. Conventional couplers do not have such a wide bandwidth; however, a low-pass filter at the output of each HPA generally removes the harmonics. Thus, the harmonics at output ports in this HPA array are not taken into account. Fig. 3 shows an N-element balanced HPA array with IM controllers. The controllers can control the amplitude and phase of the IM3s alone, with small influence on the carriers. If the IM amplitudes and phases can be randomized, the IMs are spread to all the output ports from OP_1 to OP_N. When the carriers are input to the input port $\mathrm{IP}_M (1 \leq M \leq N)$, the output spectra of the output port OP_M contain: 1) the amplified carriers that are input from the input port IP_M and 2) the generated IMs in all HPAs. In this case, carrier power is increased by voltage summation at the output port OP_M. However, IM power is distributed to all the output ports. As a result, IM controller improves the carrier power to third-order intermodulation power ratio (C/IM3) at port OP_M. The combined carrier and IM powers can be expressed by the following equations:

$$P_C\ (\mathrm{dBm}) = p_C\ (\mathrm{dBm}) + 10\log N\ (\mathrm{dBm}) \tag{1}$$

$$\begin{aligned} P_{\mathrm{IM}}\ (\mathrm{dBm}) &= \big(p_{\mathrm{IM}}\ (\mathrm{dBm}) + 10\log N\ (\mathrm{dBm})\big) \\ &\quad - 10\log N\ (\mathrm{dBm}) \end{aligned} \tag{2}$$

where P_C is the carrier output power at the output port, P_{IM} is the IM output power at the output port, p_C is the carriers' output power of an HPA, p_{IM} is the IM output power of an HPA, and N is the number of HPAs.

Therefore, the C/IM is expressed as follows:

$$\begin{aligned} (\mathrm{C/IM})_{\mathrm{array}} &= P_C - P_{\mathrm{IM}} \\ &= (p_C + 10\log N) - p_{\mathrm{IM}} \\ &= (p_C - p_{\mathrm{IM}}) + 10\log N \\ &= (\mathrm{C/IM})_{\mathrm{HPA}} + 10\log N \end{aligned} \tag{3}$$

where $(\mathrm{C/IM})_{\mathrm{array}}$ is the C/IM of the HPA array at the output port in decibels and p_C and $(\mathrm{C/IM})_{\mathrm{HPA}}$ are the C/IMs of a single HPA in decibels. Consequently, the improvement in the C/IM becomes $10\log N$.

III. IM Controller

To achieve the $(\mathrm{C/IM})_{\mathrm{array}}$ improvement calculated in (3), IM controllers should control IMs generated in each HPA to dissolve the relationship with carriers. The required functions for the IM controller are: 1) IM phase control with small influence on carriers and 2) IM amplitude control with small influence on carriers. Our developed even-order distortion implemented intermodulation distortion controller (EODIC) satisfies these requirements. We introduced the EODIC as a new linearizer [8]. It can compensate the HPA in the S-band at a lower OBO level than the conventional linearizer. The EODIC showed high IM control performance [9], [10]. A block diagram of the EODIC is shown in Fig. 4. It consists of a two-way power divider, a variable phase shifter (VPS), a frequency doubler, two variable-gain amplifiers (VGA1 and VGA2), an amplitude modulator (AM), and an output-buffer amplifier.

When two-tone carriers with frequencies ω_1 and ω_2 are input to the EODIC, the input carriers $C_{2\mathrm{tone}}$ are described as

$$C_{2\mathrm{tone}} = A\sin(\omega_1 t + \phi_1) + A\sin(\omega_2 t + \phi_2) \tag{4a}$$

where A is the amplitude of each carrier, and ϕ_1 and ϕ_2 are the initial phase of each carrier.

The input carriers are divided into a linear and nonlinear path. In the nonlinear path, the carriers' phases are shifted by a VPS, and the carriers' amplitude is controlled by VGA1. Then

$$\begin{aligned} C_{\mathrm{nonlin}} &= A'\Big\{\sin\Big(\omega_1 t + \phi_1' + \Delta\phi_1^{\mathrm{VPS}}\Big) \\ &\qquad + \sin\Big(\omega_2 t + \phi_2' + \Delta\phi_2^{\mathrm{VPS}}\Big)\Big\} \\ A' &= f_1(A, V_1) \end{aligned} \tag{4b}$$

where C_{nonlin} is the output carriers of VGA1, and A' is the amplitude of each carrier at the output point of VGA1 and gain function of V_1. The control voltage of VGA1, ϕ_1', and ϕ_2' is the phase of each signal at the output point of VPS, of which each phase depends on the electrical length and cannot be controlled by the VPS, and $\Delta\phi_1^{\mathrm{VPS}}$ and $\Delta\phi_2^{\mathrm{VPS}}$ are the amount of phase shift controlled by the VPS.

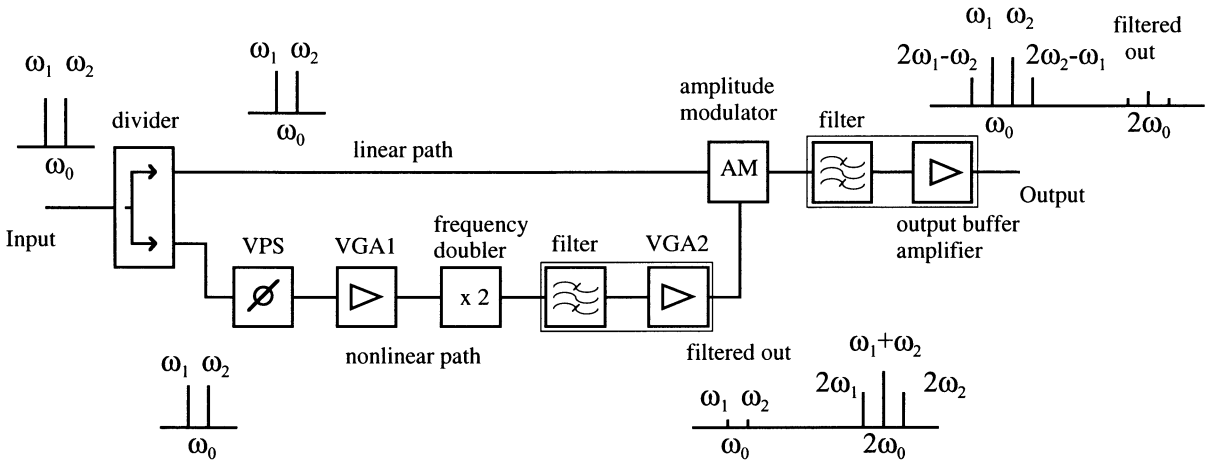

Fig. 4. Block diagram of the EODIC and the relationship of spectra when two-tone carriers (ω_1, ω_2) are input to the EODIC.

The carriers in the nonlinear path are then converted to second-order harmonics $\mathrm{IM}_{2\mathrm{ndf}}$ by the frequency doubler

$$\begin{aligned}\mathrm{IM}_{2\mathrm{ndf}} &= \alpha A'^2 \Big\{\sin\Big(\omega_1 t + \phi_{21} + \Delta\phi_1^{\mathrm{VPS}}\Big) \\ &\quad + \sin\Big(\omega_2 t + \phi_{22} + \Delta\phi_2^{\mathrm{VPS}}\Big)\Big\}^2 \\ &= \alpha A'^2 \Big\{\sin^2\Big(\omega_1 t + \phi_{21} + \Delta\phi_1^{\mathrm{VPS}}\Big) \\ &\quad + \sin^2\Big(\omega_2 t + \phi_{22} + \Delta\phi_2^{\mathrm{VPS}}\Big) \\ &\quad + 2\sin\Big(\omega_1 t + \phi_{21} + \Delta\phi_1^{\mathrm{VPS}}\Big) \\ &\quad \times \sin\Big(\omega_2 t + \phi_{22} + \Delta\phi_2^{\mathrm{VPS}}\Big)\Big\} \\ &= \frac{\alpha A'^2}{2}\Big\{\cos\Big(2\omega_1 t + 2\phi_{21} + 2\Delta\phi_1^{\mathrm{VPS}}\Big) \\ &\quad + \cos\Big(2\omega_2 t + 2\phi_{22} + 2\Delta\phi_2^{\mathrm{VPS}}\Big) - 2 \\ &\quad + 2\cos\Big((\omega_1+\omega_2)t + \phi_{21} + \phi_{22} + \Delta\phi_1^{\mathrm{VPS}} \\ &\qquad + \Delta\phi_2^{\mathrm{VPS}}\Big) \\ &\quad - 2\cos\Big((\omega_2-\omega_1)t - \phi_{21} + \phi_{22} \\ &\qquad -\Delta\phi_1^{\mathrm{VPS}} + \Delta\phi_2^{\mathrm{VPS}}\Big)\Big\} \end{aligned} \tag{4c}$$

where α is the conversion factor of the frequency doubler, and ϕ_{21} and ϕ_{22} is the phase of each signal at the output point of the frequency doubler, of which each phase depends on the electrical length of the path.

Equation (4c) contains dc, the harmonics $\omega_2 - \omega_1$, and the second-order harmonics $2\omega_1$, $\omega_1 + \omega_2$, and $2\omega_2$. The dc and distortions in the low-frequency band $\omega_2 - \omega_1$ are filtered out by VGA2. Additionally, VGA2 can control the amplitude of $\mathrm{IM}_{2\mathrm{ndf}}$ by VGA2 control voltage V_2. Thus, $\mathrm{IM}_{2\mathrm{ndf}}$ is expressed as $\mathrm{IM}'_{2\mathrm{ndf}}$ as follows:

$$\begin{aligned}\mathrm{IM}'_{2\mathrm{ndf}} &= A\Big\{\cos\Big(2\omega_1 t + 2\phi_{21} + 2\Delta\phi_1^{\mathrm{VPS}}\Big) \\ &\quad + \cos\Big(2\omega_2 t + 2\phi_{22} + 2\Delta\phi_2^{\mathrm{VPS}}\Big) \\ &\quad + 2\cos\Big((\omega_1+\omega_2)t + \phi_{21} + \phi_{22} \\ &\qquad + \Delta\phi_1^{\mathrm{VPS}} + \Delta\phi_2^{\mathrm{VPS}}\Big)\Big\} \\ A &= f_2(A', V_2, \alpha). \end{aligned} \tag{4d}$$

In practice, leaked input signals are contained in the output spectra of the frequency doubler. However, these components are also filtered out.

The AM causes IMs to be generated in the fundamental frequency band

$$\begin{aligned}\mathrm{AM}_{\mathrm{out}} &= C_{\mathrm{lin}}\Big(K + \beta \cdot IM'_{2\mathrm{ndf}}\Big) \\ &= K \cdot C_{\mathrm{lin}} + \beta \cdot C_{\mathrm{lin}} \cdot IM'_{2\mathrm{ndf}} \end{aligned} \tag{4e}$$

where $\mathrm{AM}_{\mathrm{out}}$ is the output of the AM, C_{lin} is the input carriers of the AM via the linear path, K is a factor of C_{lin}, which has an almost constant value, β is a modulation factor, which depends on the amplitudes and phases of C_{lin} and $\mathrm{IM}'_{2\mathrm{ndf}}$ and on the characteristics of the AM, such as added voltage. Here, $\mathrm{AM}_{\mathrm{out}}$ consists of two terms. The first term is the carriers and the second term is the odd-order distortion. The third-order distortions in the second term $\mathrm{IM3}_{\mathrm{fundf}}$ are given as follows:

$$\begin{aligned}\mathrm{IM3}_{\mathrm{fundf}} &= \beta \cdot C_{\mathrm{lin}} \cdot \mathrm{IM}'_{2\mathrm{ndf}} \\ &= A'''\Big\{\sin\Big(\omega_1 t + \phi_{31} + 2\Delta\phi_1^{\mathrm{VPS}}\Big) \\ &\quad + \sin\Big(\omega_2 t + \phi_{32} + 2\Delta\phi_2^{\mathrm{VPS}}\Big) \\ &\quad + 2\sin\Big(\omega_1 t + \phi_{33} + \Delta\phi_1^{\mathrm{VPS}} + \Delta\phi_2^{\mathrm{VPS}}\Big) \\ &\quad + 2\sin\Big(\omega_2 t + \phi_{34} + \Delta\phi_1^{\mathrm{VPS}} + \Delta\phi_2^{\mathrm{VPS}}\Big) \\ &\quad + \sin\Big((2\omega_1-\omega_2)t + \phi_{35} + 2\Delta\phi_1^{\mathrm{VPS}}\Big) \\ &\quad + \sin\Big((2\omega_2-\omega_1)t + \phi_{36} \\ &\qquad +2\Delta\phi_2^{\mathrm{VPS}}\Big)\Big\} \end{aligned} \tag{4f}$$

$$\begin{aligned} A''' &= f_3(A, A'', \beta) \\ &= f_3(A, V_1, V_2, \alpha, \beta). \end{aligned} \tag{4g}$$

The amplitude of $\mathrm{IM3}_{\mathrm{fundf}}$, A''', can be controlled by V_1 and V_2, which are control voltages of VGA1 and VGA2, the frequency doubler, and the AM in the EODIC, as expressed by (4g). Also, $\phi_{3m}(1 \le m \le 6)$ are phases of each signal, of which each phase depends on the electrical length of the divider, linear path, nonlinear path, and AM, and cannot be controlled by the VPS.

The wireless communication system considered here is narrow-band and, in this case, for the VPS phase shift, it can be assumed that $\Delta\phi_1^{\mathrm{VPS}} \cong \Delta\phi_2^{\mathrm{VPS}}$. This assumes

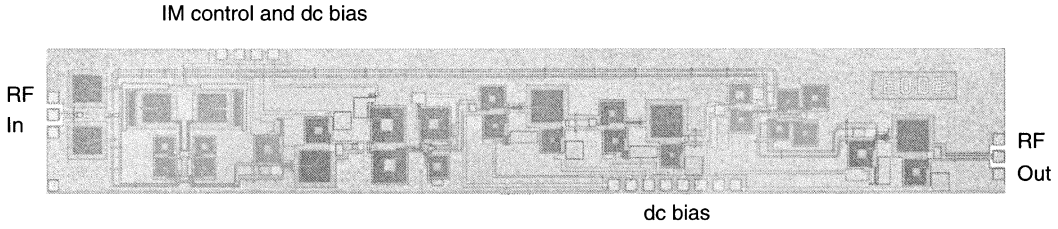

Fig. 5. Microphotograph of an EODIC fabricated on a GaAs monolithic microwave integrated circuit (MMIC). The chip measures 1.1 mm × 8.0 mm.

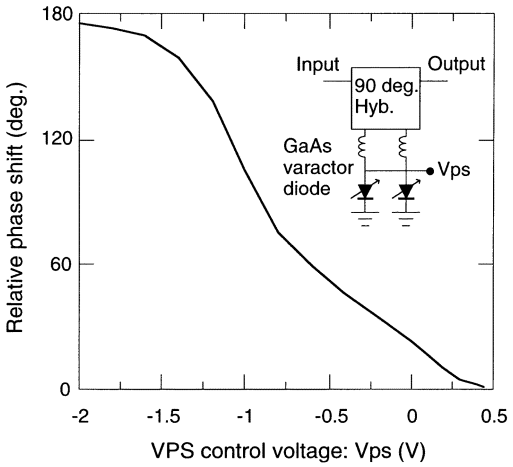

Fig. 6. Measured phase control performance of the VPS.

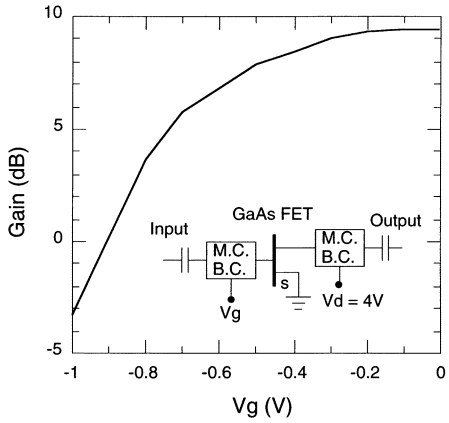

Fig. 7. Measured gain control performance of VGA1.

$\Delta\phi_1^{\mathrm{VPS}} = \Delta\phi_2^{\mathrm{VPS}} = \Delta\phi^{\mathrm{VPS}}$ and also assumes $\phi_{33} \cong \phi_{31}$ and $\phi_{34} \cong \phi_{32}$ and, thus, (4f) is represented as

$$\begin{aligned}\mathrm{IM3}_{\mathrm{fundf}} = A'''\Big\{&3\sin\left(\omega_1 t + \phi_{31} + 2\Delta\phi^{\mathrm{VPS}}\right)\\ &+ 3\sin\left(\omega_2 t + \phi_{32} + 2\Delta\phi^{\mathrm{VPS}}\right)\\ &+ \sin\left((2\omega_1 - \omega_2)t + \phi_{35} + 2\Delta\phi^{\mathrm{VPS}}\right)\\ &+ \sin\left((2\omega_2 - \omega_1)t + \phi_{36} + 2\Delta\phi^{\mathrm{VPS}}\right)\Big\}.\end{aligned} \tag{4h}$$

Therefore, when the VPS can control the phase from 0° to 180°, the phase of $\mathrm{IM3}_{\mathrm{fundf}}$ can be controlled from 0° to 360°.

In conventional linearizers, carriers in the linear path are affected by carriers leaking from the nonlinear path. In EODICs, the leaking carriers can be filtered out so that they will not affect the carriers in the linear path. Therefore, EODICs have advantageous distortion control performance.

IV. Control Performance

The fabricated prototype EODIC was examined using a microwave wafer probe station. Fig. 5 shows a prototype EODIC fabricated on a GaAs chip. The VPS is composed of a 3-dB 90° hybrid coupler, two inductors, and two GaAs varactor diodes. The measured phase control performance of the VPS is shown in Fig. 6. It can be controlled by about 180°. The VGA1 is composed of a source-grounded GaAs FET, matching circuits, and bias circuits. The measured gain control performance achieved by controlling the gate bias is shown in Fig. 7. Since VGA2 has the same circuit structure as VGA1, it shows similar gain control performance.

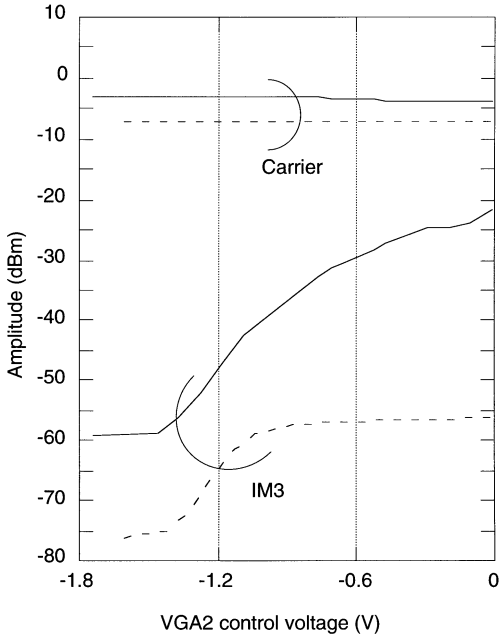

Fig. 8. Amplitude control performance of the EODIC. The solid lines designate $\mathrm{Pin} = -5$ dBm/tone, and the dotted lines designate $\mathrm{Pin} = -10$ dBm/tone.

The EODIC was tested with a two-tone carrier input of $f_1 = 2.517$ GHz and $f_2 = 2.518$ GHz. In this case, the EODIC generates two IM3s of 2.516 and 2.519 GHz. Figs. 8 and 9 show the measured carrier data of 2.517 GHz and IM3 data of 2.516 GHz. The total gain was approximately 2 dB for the carriers. The IM3 amplitudes versus VGA2 control voltage was measured using a spectrum analyzer, as is plotted in Fig. 8, for an input power of −5 dBm/tone (solid line) and −10 dBm/tone (dotted line). This

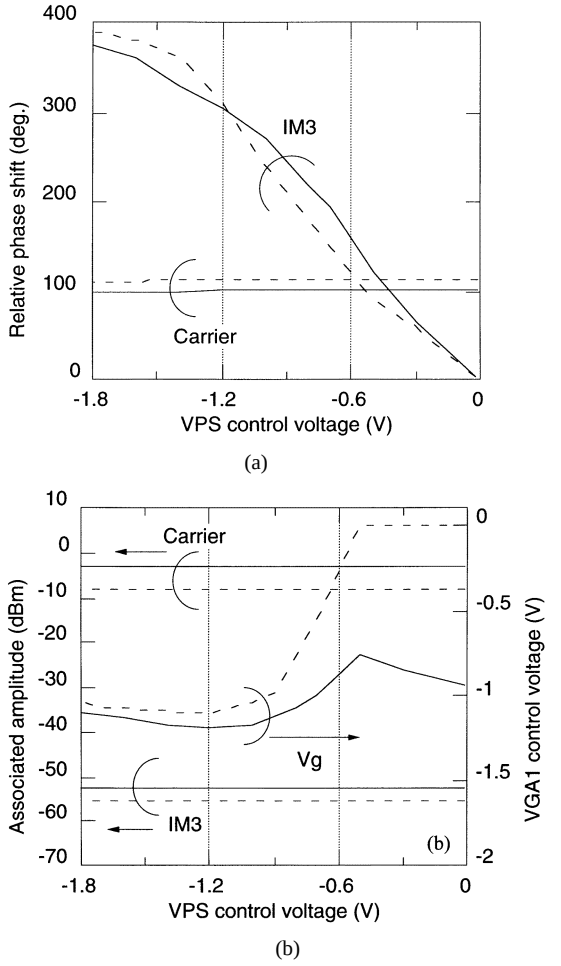

Fig. 9. Phase control performance of an EODIC. The solid lines designate $\mathrm{Pin} = -5$ dBm/tone, and the dotted lines designate $\mathrm{Pin} = -10$ dBm/tone. (a) Phase control performance. (b) Associated amplitude of phase control. The VGA1 control voltage compensates associated amplitude deviation.

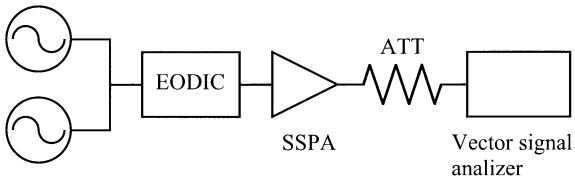

Fig. 10. Experimental setup to measure amplitude and phase of carriers and IM3s generated in the SSPA with the EODIC. Two-tone carriers are input to the EODIC. The output power and relative phase of carriers and IM3s are measured via a vector signal analyzer.

shows that, for an input power of -5 dBm/tone, the IM3 amplitude was successfully controlled over a 35-dB range, while the carriers kept a quite constant amplitude, deviating by only 1 $\mathrm{dB_{p-p}}$. In addition, for an input power of -10 dBm/tone, the IM3 amplitude was controlled over a 20-dB range, while the carriers again kept a quite constant amplitude, deviating by only 0.1 $\mathrm{dB_{p-p}}$.

The measured relative phase versus VPS control voltage is shown in Fig. 9(a). The solid lines again designate $\mathrm{Pin} = -5$ dBm/tone, and the dotted lines designate $\mathrm{Pin} = -10$ dBm/tone. It can be seen that the IM3 phase was controlled over a range of over 360° by the VPS voltage, while the carrier kept an almost constant phase with a very

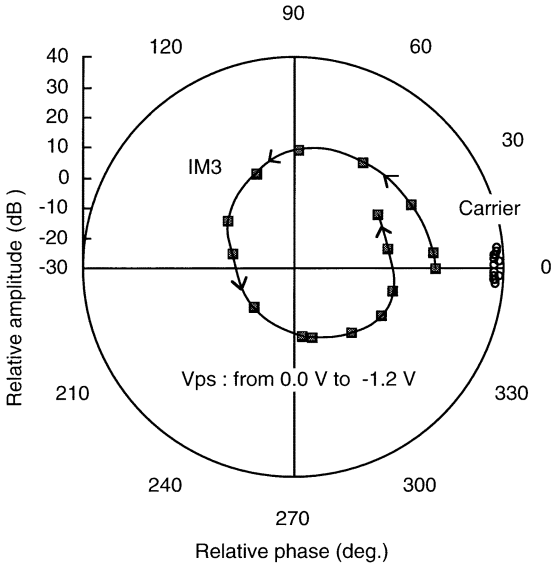

Fig. 11. Phase control performance of the carrier and IM3 in an SSPA controlled by an EODIC.

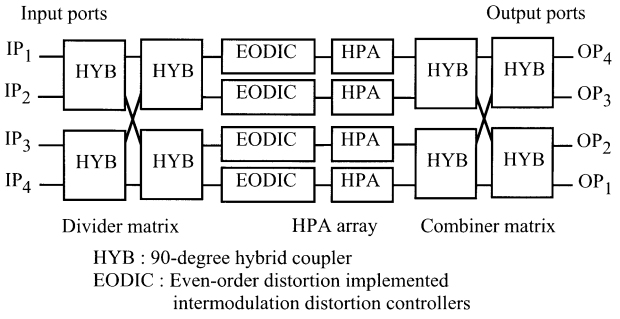

Fig. 12. Block diagram of a four-element HPA array.

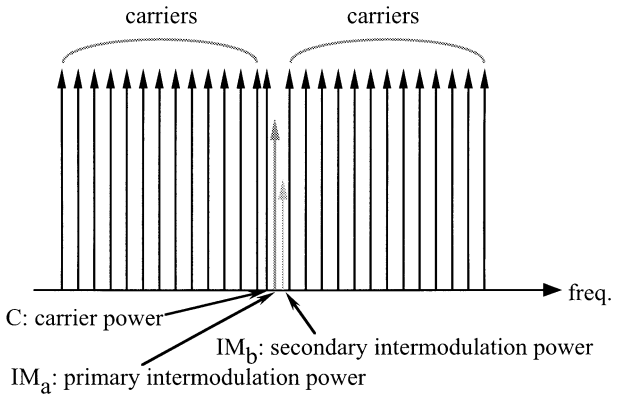

Fig. 13. Output spectra in 27-tone evaluation.

small change of only $2^{\circ}_{\mathrm{p-p}}$. The phase control unfortunately produces some amplitude perturbation due to the presence of parasitic elements and the limited input-to-output isolation of the VPS. To overcome the perturbation, the VGA1 control voltage is adjusted in accordance with the VPS control voltage. This successfully compensates for the carrier and IM3 amplitude deviations. As shown in Fig. 9(b), the carrier and IM3 amplitudes are quite constant, deviating by only 0.3 $\mathrm{dB_{p-p}}$. The carriers in Figs. 8 and 9 include the fundamental components that depend on the control voltage of VPS, VGA1, and

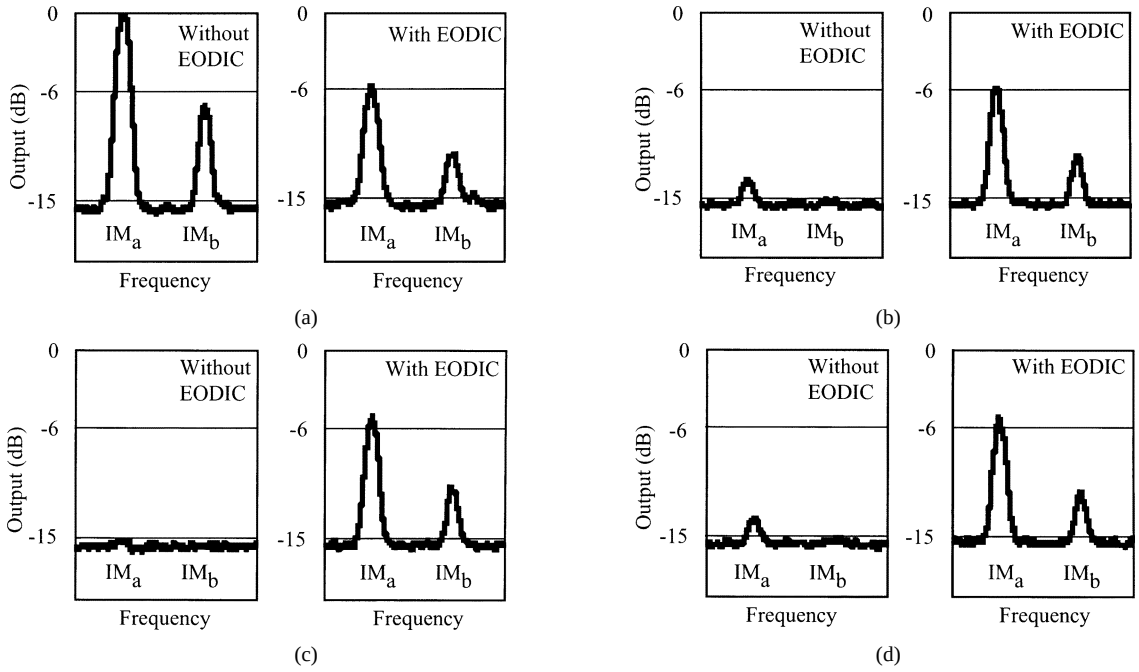

Fig. 14. Output spectra of combiner matrix. (a) Output port OP_1, (b) Output port OP_2, (c) Output port OP_3. (d) Output port OP_4. Those with (without) an EODIC are shown on the right-hand (left-hand) side. The vertical axes plot output power (in decibels) relative to the maximum power of IM_a.

VGA2, as shown in (4h). When the C/IM3 was over 30 dB, the influence of the control voltages of VPS, VGA1, and VGA2 was minimal. However, when the C/IM3 was smaller than 25 dB, the influence was recognized as carrier amplitude deviation, as shown in Fig. 8.

We used a 20-W-class SSPA and a vector signal analyzer to evaluate the amplitude and phase control performance of the IM3s generated in the SSPA with an EODIC. The experimental setup is shown in Fig. 10. The measured amplitude and relative phase of the carrier and the IM3s generated in the SSPA with an EODIC are shown in the polar graphs in Fig. 11, when the output OBO level is 5.5 dB. The IM3s were controlled over a range of over 360° in-phase, while the carriers' amplitudes and phases were maintained almost constant.

The results confirmed that good control characteristics were obtained in terms of IM amplitude and phase, while those of the carriers were kept nearly constant. The IM control achieved with an EODIC has little influence on the carriers, which is an advantage over conventional linearizers. An EODIC can be applied to the IM control technique proposed in Section II.

V. Experimental Results of HPA Array

The proposed IM control technique was demonstrated experimentally using a four-element HPA array comprising 20-W-class SSPAs in the S-band. The key to the proposed technique is that IM is controlled independently of the carriers. An experimental block diagram is shown in Fig. 12. An EODIC was located in front of each HPA. In this experiment, multitone (27-tone) carriers were used to evaluate the effect of the higher order distortion products. The number of higher order distortion products increases with the number of carriers because the products are produced from the combination of carriers. The 27-tone carriers were located as shown in Fig. 13. All carriers were spaced equally, except for the center carrier. The center-carrier frequency was shifted to a slightly lower frequency to measure the IM_a and IM_b. The C/IM of the 27-tone carriers, $(\mathrm{C/IM})_{\mathrm{multi}}$ in dB, is given by

$$(\mathrm{C/IM})_{\mathrm{multi}} = C - 10\log\left(10^{(\mathrm{IM}_a/10)} + 10^{(\mathrm{IM}_b/10)}\right). \quad (5)$$

The 27-tone carriers are modulated by QPSK. The bandwidth is 35 MHz in the S-band. The center frequency is 2.518 GHz and the frequency spacing is 1.35 MHz. Output spectra of the combiner matrix are shown in Fig. 14. We monitored the output spectra of all the output ports with a spectrum analyzer. The VPS control voltages were manually set to distribute IMs to all the ports. VGA1 and VGA2 were set to compensate for the loss of VPS depending on VPS control voltage. Those with (without) an EODIC are shown on the right-hand (left-hand) side. The vertical axes plot output power relative to the maximum power of IM_a. The 27-tone carriers are input from input port IP_1. Without an EODIC, IM power was concentrated at the output port OP_1, as shown in Fig. 14(a). The output spectra of IM_a and IM_b were very small at the other output ports. On the other hand, with an EODIC, IM power was evenly distributed to all ports from OP_1 to OP_4. At output port OP_1, IM power with an EODIC was 6 dB lower than for the case without an EODIC [5]. Carriers are not shown in Fig. 14; however, in both cases, with and without an EODIC, carriers had the same output power at the output port OP_1. Therefore, C/IM was improved by 6 dB from 31 to 37 dB at the output port OP_1. This result is consistent with the expected value of $(10\log 4)$ dB calculated from (3). By using the EODIC, at a C/IM ratio of 37 dB, the power-added efficiency increases from 6% to approximately 11%, which is not superior to a conventional linearizer. However, we confirmed the proposed distribution technique. Our estimated C/IM ratio requirement is above 26 dB for our planning satellite system, therefore, the proposed technique should be demonstrated in a near-saturated region. The developed EODIC did not generate

sufficient IM power; it could not control IM of a saturated HPA. A redesigned EODIC will solve the problem.

VI. Application to Phased Arrays

The proposed technique can also be adapted to an APAAS. In an APAAS, when carriers are combined in-phase, the IMs are also combined in-phase because of the association between carriers and IMs. Accordingly, carrier beam direction and IM beam direction are almost the same. On the other hand, by using an EODIC, when carriers are combined in-phase, the IMs are not combined in-phase. The carrier radiation pattern and IM radiation pattern can then be different. The IMs are controlled so that the IM controllers can treat them as a power summation, C/IM is increased along the carrier beam direction by $10 \log N$ dB. Since future communication satellite may use active phased arrays having over 100 elements, the use of the IM control technique will improve C/IM by over 20 dB $(10 \log 100)$. The improvement will help to achieve high power efficiency in HPAs and low power consumption in satellites.

VII. Conclusion

A novel concept for using IM control to increase the efficiency of an HPA array with high C/IM has been proposed. A developed EODIC has been shown to be an effective IM controller. The effect of IM control has been demonstrated in experiments using a four-element HPA array with EODICs. The obtained results show that C/IM was improved by 6 dB, i.e., from 31 to 37 dB. This is consistent with the calculated value. This technique makes it possible to achieve high efficiency in an HPA array with high C/IM to solve the heat-shedding problem expected in future communication satellites, which will output several kilowatts of RF power.

Acknowledgment

The authors would like to thank Dr. H. Mizuno, NTT Network Innovation Laboratories, NTT Corporation, Kanagawa, Japan, for his support and encouragement. The authors also thank Dr. T. Ohira, ATR Adaptive Communications Research Laboratories, Kyoto, Japan, and Y. Imaizumi, NTT Network Innovation Laboratories, NTT Corporation, and Y. Suzuki, NTT Network Innovation Laboratories, NTT Corporation, for their useful discussions.

References

[1] T. Ohira, K. Ueno, K. Horikawa, and H. Ogawa, "Onboard active phased array techniques for high-performance communication satellites," in *Proc. IEICE Microwave Eng.*, 1997, pp. 339–345.

[2] T. Ono *et al.*, "Linearized C-band SSPA incorporating dynamic bias operation for GLOBALSTAR," in *Proc. AIAA 16th Int. Solid-State Circuits Conf.*, 1996, pp. 123–130.

[3] M. Sigaki *et al.*, "S-band high-power and high-efficiency SSPA for on boarding satellite," in *Proc. AIAA 16th Int. Solid-State Circuits Conf.*, 1996, pp. 108–112.

[4] S. Torrents, J. Baucells, and J. Martinez, "An internally tuned Ku-band monolithic predistortion linearizer," in *Proc. 26th Eur. Microwave Conf.*, 1996, pp. 204–207.

[5] S. Narahashi and T. Nojima, "Non-linear distortion compensation techniques of power amplifiers for mobile communication systems," in *Proc. IEICE Microwave Eng.*, 1997, pp. 87–92.

[6] N. Imai, T. Nojima, and T. Murase, "Novel linearizer using balanced circulators and its application to multilevel digital radio systems," *IEEE Trans. Microwave Theory Tech.*, vol. 37, pp. 1237–1243, Aug. 1989.

[7] Y. Nakasuga, T. Kaho, and K. Horikawa, "A novel technique based on power combining mechanism that yields HPA arrays with high power efficiency," in *Proc. IEEE Phased Array Syst. and Technol.*, 2000, pp. 129–132.

[8] K. Horikawa and H. Ogawa, "Even-order distortion enveloping method to linearizer saturated high power amplifiers," in *Proc. IEEE MTT-S Int. Technol. Wireless Applicat. Symp.*, 1997, pp. 79–82.

[9] T. Kaho, H. Okazaki, and T. Ohira, "A GaAs monolithic intermodulation controller for active phased array systems," in *Proc. APMC'98*, pp. 603–606.

[10] T. Kaho, H. Okazaki, K. Horikawa, K. Araki, and T. Ohira, "Improvement technique in the C/I of a high-power-amplifier array using intermodulation distortion controllers," in *Proc. RAWCON'99*, pp. 183–186.

Takana Kaho was born in Sapporo, Japan, in 1971. She received the B.S. and M.S. degrees in physics from the Tokyo Metropolitan University, Tokyo, Japan, in 1994 and 1996, respectively.

In 1996, she joined NTT Wireless Communication System Laboratories (now NTT Network Innovation Laboratories), NTT Corporation, Yokosuka, Japan, where she has been engaged in research of satellite on-board amplifier.

Ms. Kaho is a member of the Institute of Electronics, Information and Communication Engineers (IEICE), Japan. She was the recipient of the 1998 Japan Microwave Prize presented at the Asia–Pacific Microwave Conference.

Yoshinori Nakasuga was born in Nagasaki, Japan, in 1966. He received the B.E. and M.S. degrees in physics from Okayama University, Okayama, Japan, in 1989 and 1991, respectively.

In 1991, he joined NTT Wireless Communication Systems Laboratories (now NTT Network Innovation Laboratories), NTT Corporation, Yokosuka, Japan, where he is engaged in research on satellite communication systems.

Mr. Nakasuga is member of the Institute of Electronics, Information and Communication Engineers (IEICE), Japan.

Hiroshi Okazaki (A'94–M'00) received the B.E. and M.E. degrees from Osaka University, Osaka, Japan, in 1988 and 1990, respectively.

In 1990, he joined the NTT Radio Communication Systems Laboratories (now NTT Network Innovation Laboratories), Kanagawa, Japan, where he was involved in research on power and size minimization techniques for microwave circuits and equipments. Since April 2001, he has been with the NTT Electronics (NEL) Corporation, Machida, Japan, where he is currently an Engineering Manager in the Integrated Circuit Design Department, involved in the development of ultra-high-speed devices for photonic communication systems.

Mr. Okazaki was the recipient of the 1997 Young Engineer Award presented by the Institute of Electronics, Information and Communication Engineers (IEICE), Japan, and the 1998 Japan Microwave Prize.

Katsuhiko Araki received the B.E. and M.E. degrees from the Tokyo Institute of Technology, Tokyo, Japan, in 1979 and 1981, respectively.

In 1981, he joined the NTT Electrical Communications Laboratories, Yokosuka, Japan, where he was engaged in research on GaAs monolithic microwave circuits and the development of communication satellite on-board transponders. He is currently a Senior Research Engineer, Supervisor with NTT Network Innovation Laboratories, Kanagawa, Japan.

Mr. Araki is a member of the American Institute of Aeronautics and Astronautics (AIAA) and the Institute of Electronics, Information and Communication Engineers (IEICE), Japan. He was the recipient of the 1988 IEEE Sinohara Prize.

Kohji Horikawac (M'93) received the B.S. degree in electrical engineering from the Tokyo Institute of Technology, Tokyo, Japan, in 1984.

In 1984, he joined the Yokosuka Electrical Communication Laboratories, NTT Research and Development Bureau, where he was engaged in research and development of satellite on-board transponders. From 1993 to 1997, he was involved with research on optical/microwave interaction systems and photonic beam-forming networks for microwave active phased-array antennas. He is currently an Executive Engineer with the Radio Network Development Department, NTT DoCoMo Inc., Yokosuka, Japan.

Mr. Horikawa is a member of the Institute of Electronics, Information and Communication Engineers (IEICE), Japan.